

# Synthetic free-oscillation spectra: an appraisal of various mode-coupling methods

Hsin-Ying Yang<sup>1,2</sup> and Jeroen Tromp<sup>2,3</sup>

<sup>1</sup>Department of Geosciences, National Taiwan University, Taipei 106, Taiwan. E-mail: [hsinyingTW@gmail.com](mailto:hsinyingTW@gmail.com)

<sup>2</sup>Department of Geosciences, Princeton University, Princeton, NJ 08544, USA

<sup>3</sup>Program in Applied and Computational Mathematics, Princeton University, Princeton, NJ 08544, USA

Accepted 2015 August 17. Received 2015 August 17; in original form 2015 July 10

## SUMMARY

Normal-mode spectra may be used to investigate large-scale elastic and anelastic heterogeneity throughout the entire Earth. The relevant theory was developed a few decades ago, however—mainly due to computational limitations—several approximations are commonly employed, and thus far the full merits of the complete theory have not been taken advantage of. In this study, we present an exact algebraic form of the theory for an aspherical, anelastic and rotating Earth model in which either complex or real spherical harmonic bases are used. Physical dispersion is incorporated into the quadratic eigenvalue problem by expanding the logarithmic frequency term to second-order. Proper (re)normalization of modes in a 3-D Earth model is fully considered. Using a database of 41 earthquakes and more than 10 000 spectra containing 116 modes with frequencies less than 3 mHz, we carry out numerical experiments to quantitatively evaluate the accuracy of commonly used approximate mode synthetics. We confirm the importance of wideband coupling, that is, fully coupling all modes below a certain frequency. Neither narrowband coupling, in which nearby modes are grouped into isolated clusters, nor self-coupling, that is, incorporating coupling between singlets within the same multiplet, are sufficiently accurate approximations. Furthermore, we find that (1) effects of physical dispersion can be safely approximated based on either a fiducial frequency approximation or a quadratic approximation of the logarithmic dispersion associated with the absorption-band model; (2) neglecting the proper renormalization of the modes of a rotating, anelastic Earth model introduces only minor errors; (3) ignoring the frequency dependence of the Coriolis and kinematic matrices in a wideband coupling scheme can lead to  $\sim 6$  per cent errors in mode spectra at the lowest frequencies; notable differences also occur between narrowband coupling and quasi-degenerate perturbation theory, which linearizes the eigenvalue problem as well.

**Key words:** Tomography; Surface waves and free oscillations; Computational seismology; Theoretical seismology.

## 1 INTRODUCTION

Earth's free oscillations are generated by large ( $M_w > 8$ ) earthquakes and their signals can last for hundreds of hours. Collectively, these long-period normal modes are sensitive to large-scale variations in shear and compressional wave speeds, density, anisotropy and attenuation throughout our entire planet. Analysing free oscillation spectra can help shed light on several controversial issues, such as the presence of thermally or/and chemically distinct large low-shear velocity provinces (LLSVPs) underneath South Africa and the Pacific (Ishii & Tromp 1999), hemispherical variations in inner core anisotropy (Deuss *et al.* 2010) and the existence of an innermost inner core (Ishii & Dziewonski 2002). This paper is con-

cerned with the accurate calculation of synthetic free oscillation spectra.

Early normal-mode theories focused on the effects of the Earth's rotation and ellipticity on free oscillation spectra. Based on Rayleigh's principle, Dahlen (1968) considered the effects of rotation and ellipticity on mode frequencies. The possibility of strong coupling between nearly resonant modes, particularly between certain toroidal and spheroidal modes, was pointed out by Dahlen (1969), but not until Woodhouse (1980) was the effect of attenuation on coupled modes investigated. Dahlen & Smith (1975) noted the non-orthogonal properties of the eigensolutions of a rotating Earth model, an issue confirmed numerically by Park & Gilbert (1986) based on a Galerkin method. The proper normalization of

the modes of a rotating anelastic Earth model was first discussed by Lognonné (1991).

Although normal-mode theory was well established by the 1990s, computational limitations hampered its full practical applications. Since solving the normal-mode eigenvalue problem involves diagonalizing a huge matrix, several alternatives were proposed to improve computational efficiency. The subspace projection method (Dahlen 1987; Park 1987, 1990; Um & Dahlen 1992) considered exact coupling within a target multiplet by invoking the Galerkin method for matrices of small size, while truncating coupling interactions between multiplets. Lognonné (1991) presented a similar approach based on higher-order perturbation theory. More recently, an iterative method was developed by Deuss & Woodhouse (2004). Different from the approach of Lognonné (1991), which only updates eigenmodes twice, this method iteratively improves eigenmodes as many times as needed until convergence so as to capture the exact solution. The work of Deuss & Woodhouse (2001) makes it practical to compute wideband synthetics up to 3 mHz based on the brute-force diagonalization of matrices. One potential limitation of the Deuss & Woodhouse (2001) approach is that logarithmic physical dispersion due to intrinsic attenuation is approximated, something we investigate in this study. As an alternative to solving eigenvalue problems, the direct solution method (Hara *et al.* 1993; Al-Attar *et al.* 2012) fully considers wideband coupling and accommodates anelasticity without approximation.

Strong coupling is frequently confined to singlets within a single multiplet or to singlets comprising a handful of coupled multiplets (e.g. Park 1990). Motivated by this observation, one may solely consider coupling within an individual multiplet (e.g.  ${}_0S_2$ ) or among a small group of multiplets (e.g.  ${}_0S_2 \rightarrow T_2 \rightarrow S_1$ ) around a suitably chosen fiducial frequency. In these approximations, the nonlinear eigenvalue problem governing the oscillations may be reduced to a standard linear eigenvalue problem based on (quasi-)degenerate perturbation theory (e.g. Luh 1974; Tromp & Dahlen 1990; Um & Dahlen 1992). Normal-mode splitting may be visualized based on the so-called ‘splitting functions’ (e.g. Giardini *et al.* 1988; Resovsky & Ritzwoller 1998; Deuss *et al.* 2013), which are maps representing a radial average of Earth’s 3-D heterogeneity. It should be noted that splitting functions are determined based on self or group coupling approximations, and proper (re)normalization of modes according to the theory developed by Lognonné (1991) is frequently neglected.

In this study, we begin by summarizing an algebraic normal-mode theory for a general Earth model—including rotation, ellipticity, anelasticity and lateral heterogeneity—based on either complex or real spherical harmonics. Thanks to progress in fast numerical methods, it has become practical to diagonalize thousands-by-thousands matrices to obtain ‘exact’ synthetics. Such exact normal-mode spectra calculated based on wideband coupling up to 3 mHz are compared with results from narrowband coupling, as well as results based on quasi-degenerate perturbation theory. Finally, we discuss popular approximations that reduce mode coupling to a linear eigenvalue problem, and we investigate the effects of proper (re)normalization on synthetic spectra.

## 2 THEORY

### 2.1 Governing equations for an aspherical, anelastic and rotating Earth model

In this section, we briefly summarize the equations of motion for a self-gravitating, rotating and anelastic Earth model using the

**Table 1.** Eigensolutions and eigenfrequencies of the Earth and the anti-Earth; the latter has the opposite sense of rotation.

	$\nu$	$-\nu^*$
Earth	$\mathbf{s}$	$\mathbf{s}^*$
Anti-Earth	$\bar{\mathbf{s}}$	$\bar{\mathbf{s}}^*$

notation in section 6.3 of Dahlen & Tromp (1998). The frequency-domain momentum equation may be written in the form

$$\mathcal{H}(\nu) \mathbf{s} + 2i\nu \boldsymbol{\Omega} \times \mathbf{s} - \nu^2 \mathbf{s} = \mathbf{0}, \quad (1)$$

where  $\mathbf{s}$  denotes an eigensolution with associated complex eigenfrequency  $\nu = \omega + i\gamma$ ,  $\omega > 0$ . The integro-differential operator  $\mathcal{H}$  captures anelastic, gravitational and centrifugal effects, and  $\boldsymbol{\Omega}$  denotes angular velocity. The complex modulus  $\Lambda(\nu)$  characterizing anelasticity has the symmetry  $\Lambda^*(\nu) = \Lambda(-\nu^*)$  (Nowick & Berry 1972), and thus  $\mathcal{H}$  satisfies the relation (Dahlen 1981)

$$\mathcal{H}^*(\nu) = \mathcal{H}(-\nu^*), \quad (2)$$

where  $*$  denotes complex conjugation. Additionally,  $\mathcal{H}^*(\nu)$  is the adjoint operator of  $\mathcal{H}(\nu)$  (see eq. A4) due to the thermodynamic symmetries of  $\Lambda(\nu)$  (i.e.  $\Lambda_{ijkl} = \Lambda_{klij}$ ). Upon taking the complex conjugate of eq. (1) and using the symmetry eq. (2), we find that  $\mathbf{s}^*$  is also an eigensolution with associated eigenfrequency  $-\nu^*$ .

Dual eigensolutions may be obtained by solving the eigenproblem (1) with a reversed sense of rotation,  $\boldsymbol{\Omega} \rightarrow -\boldsymbol{\Omega}$ , that is, (Dahlen & Smith 1975; Park & Gilbert 1986; Lognonné 1991; Dahlen & Tromp 1998)

$$\mathcal{H}(\nu) \bar{\mathbf{s}} - 2i\nu \boldsymbol{\Omega} \times \bar{\mathbf{s}} - \nu^2 \bar{\mathbf{s}} = \mathbf{0}. \quad (3)$$

Upon taking the complex conjugate of eq. (3) and using the symmetry eq. (2), we find that  $\bar{\mathbf{s}}^*$  is also an eigensolution with associated eigenfrequency  $-\nu^*$ . The properties of the regular (primary) and dual eigensolution are summarized in Table 1.

The eigenfrequency does not change with the sense of rotation, as revealed by comparison of eqs (1) and (3). There is no direct relationship between the primary and dual eigensolutions,  $\mathbf{s}$  and  $\bar{\mathbf{s}}$ , respectively. However, they do satisfy the relations

$$[\bar{\mathbf{s}}, \mathbf{s}'] = [\mathbf{s}', \bar{\mathbf{s}}], \quad (4)$$

$$[\bar{\mathbf{s}}, \mathcal{H}(\nu) \mathbf{s}'] = [\mathcal{H}(\nu) \bar{\mathbf{s}}, \mathbf{s}'] = [\mathbf{s}', \mathcal{H}(\nu) \bar{\mathbf{s}}], \quad (5)$$

$$[\bar{\mathbf{s}}, i \boldsymbol{\Omega} \times \mathbf{s}'] = -[i \boldsymbol{\Omega} \times \bar{\mathbf{s}}, \mathbf{s}'] = -[\mathbf{s}', i \boldsymbol{\Omega} \times \bar{\mathbf{s}}]. \quad (6)$$

Here we have introduced the duality product  $[\mathbf{u}, \mathbf{v}]$  of complex vectors  $\mathbf{u}$  and  $\mathbf{v}$  defined by

$$[\mathbf{u}, \mathbf{v}] = \int_{\oplus} \rho \mathbf{u} \cdot \mathbf{v} dV, \quad (7)$$

where  $\rho$  denotes mass density. Note that the duality relations (5) and (6) reflect properties of the operators  $\mathcal{H}(\nu)$  and  $i \boldsymbol{\Omega} \times$ . In the Appendix, we present an alternative derivation of the relevant equations based on the proper inner product

$$\langle \mathbf{u}, \mathbf{v} \rangle = \int_{\oplus} \rho \mathbf{u}^*(\mathbf{x}) \cdot \mathbf{v}(\mathbf{x}) dV. \quad (8)$$

By invoking eqs (4)–(6) upon the difference eq. (3),  $[\mathbf{s}'] - [\bar{\mathbf{s}}, \text{eq. (1)}]$ , we find the biorthogonality relationship

$$[\bar{\mathbf{s}}, \mathbf{s}'] - 2(\nu + \nu')^{-1} [\bar{\mathbf{s}}, i \boldsymbol{\Omega} \times \mathbf{s}'] - (\nu^2 - \nu'^2)^{-1} [\bar{\mathbf{s}}, \{\mathcal{H}(\nu) - \mathcal{H}(\nu')\} \mathbf{s}'] = 0, \quad \nu \neq \nu', \quad (9)$$

and the natural normalization of the eigensolutions is

$$[\bar{\mathbf{s}}, \mathbf{s}] - \nu^{-1} [\bar{\mathbf{s}}, i \boldsymbol{\Omega} \times \mathbf{s}] - \frac{1}{2} \nu^{-1} [\bar{\mathbf{s}}, \partial_\nu \mathcal{H}(\nu) \mathbf{s}] = 1, \quad (10)$$

in which both eigensolutions,  $\mathbf{s}$  and  $\bar{\mathbf{s}}$ , share the same eigenfrequency  $\nu$ .

## 2.2 Rayleigh–Ritz method

The Rayleigh–Ritz method may be invoked by expanding the eigensolutions of a 3-D Earth model,  $\mathbf{s}$ , as a linear combination of the eigensolutions of a spherically symmetric (1-D) Earth model,  $\mathbf{s}_s$ , that is,

$$\mathbf{s} = \sum_s q_s \mathbf{s}_s, \quad (11)$$

where the expansion coefficients  $q_s$  remain to be determined. Following the notation of Dahlen & Tromp (1998), spherically symmetric eigensolutions may be represented in terms of either complex spherical harmonics,  $Y_{\ell m}$ , or real spherical harmonics,  $\mathcal{Y}_{\ell m}$ . Radial eigenfunctions may be computed based on the software package MINEOS (Woodhouse 1988; Masters *et al.* 2007). We use subscripts  $s$  to label modes of a spherically symmetric Earth model.

Next, we seek eigensolutions for the corresponding anti-Earth. Since  $\mathbf{s}_s$  and  $\mathbf{s}_s^*$  are both eigenfunctions of a spherically symmetric Earth model with eigenfrequency  $\omega > 0$ , we choose to use  $\mathbf{s}_s^*$  as the basis functions in which to expand the eigensolutions of the anti-Earth:

$$\bar{\mathbf{s}} = \sum_s \bar{q}_s \mathbf{s}_s^*. \quad (12)$$

If the spherically symmetric eigensolutions are expanded in real spherical harmonics then  $\mathbf{s}_s^* = \mathbf{s}_s$ , but the representation eq. (12) keeps our options open.

To find the coupling coefficients  $q_s$  and  $\bar{q}_s$ , we introduce the action (e.g. Dahlen & Tromp 1998)

$$\mathcal{I} = \frac{1}{2} \{ [\bar{\mathbf{s}}, \mathcal{H}(\nu) \mathbf{s}] + [\bar{\mathbf{s}}, 2i\nu \boldsymbol{\Omega} \times \mathbf{s}] - [\bar{\mathbf{s}}, \nu^2 \mathbf{s}] \}. \quad (13)$$

Note that this is equivalent to taking the duality product of  $\bar{\mathbf{s}}$  with eq. (1). Invoking Hamilton's principle, the action  $\mathcal{I}$  is stationary ( $\delta \mathcal{I} = 0$ ) with respect to perturbations  $\delta \mathbf{s}$  and  $\delta \bar{\mathbf{s}}$  provided  $\mathbf{s}$  and  $\bar{\mathbf{s}}$ , each associated with frequency  $\nu$ , are solutions to the eigenproblems eqs (1) and (3), respectively.

Upon substituting expansions eqs (11) and (12) into the action (13), we can rewrite the action in the algebraic form

$$\mathcal{I} = \frac{1}{2} \bar{\mathbf{q}}^T [\mathbf{V}(\nu) + 2\nu \mathbf{W} - \nu^2 \mathbf{T}] \mathbf{q}, \quad (14)$$

where a superscript  $T$  denotes the transpose. The elements of the potential energy matrix,  $\mathbf{V}(\nu)$ , Coriolis matrix,  $\mathbf{W}$ , and kinematic energy matrix,  $\mathbf{T}$ , are given by

$$T_{ss'} = \int_{\oplus} \rho \mathbf{s}_s^* \cdot \mathbf{s}_{s'} dV = [\mathbf{s}_s^*, \mathbf{s}_{s'}], \quad (15)$$

$$W_{ss'} = \int_{\oplus} \rho \mathbf{s}_s^* \cdot i \boldsymbol{\Omega} \times \mathbf{s}_{s'} dV = [\mathbf{s}_s^*, i \boldsymbol{\Omega} \times \mathbf{s}_{s'}], \quad (16)$$

$$V_{ss'}(\nu) = \int_{\oplus} \rho \mathbf{s}_s^* \cdot \mathcal{H}(\nu) \mathbf{s}_{s'} dV = [\mathbf{s}_s^*, \mathcal{H}(\nu) \mathbf{s}_{s'}]. \quad (17)$$

These matrices describe coupling effects between spherical Earth modes  $s$  and  $s'$ . Consequently, a  $(2\ell + 1)$ -fold degenerate multiplet will be split into  $(2\ell + 1)$  singlets. Using algebraic notation, the

normalization of an eigensolution (eq. 10) may be rewritten as

$$\bar{\mathbf{q}}^T [\mathbf{T} - \nu^{-1} \mathbf{W} - \frac{1}{2} \nu^{-1} \partial_\nu \mathbf{V}(\nu)] \mathbf{q} = 1. \quad (18)$$

Stationarity of the action eq. (14) ( $\delta \mathcal{I} = 0$ ) due to perturbations  $\delta \mathbf{q}$  and  $\delta \bar{\mathbf{q}}$  implies the left and right eigenvalue problems

$$\bar{\mathbf{q}}^T [\mathbf{V}(\nu) + 2\nu \mathbf{W} - \nu^2 \mathbf{T}] = \mathbf{0}, \quad (19)$$

$$[\mathbf{V}(\nu) + 2\nu \mathbf{W} - \nu^2 \mathbf{T}] \mathbf{q} = \mathbf{0}, \quad (20)$$

respectively. Note that, in general, due to the frequency dependence of the potential energy matrix  $\mathbf{V}$ , these constitute difficult-to-solve nonlinear eigenvalue problems.

Rather than solving the left eigenvalue problem (eq. 19), for which few solvers are available even for linear or quadratic eigenvalue problems, we derive an auxiliary system of which  $\bar{\mathbf{q}}$  is the right eigenvector. Depending on the choice of real versus complex spherical harmonics, this auxiliary system takes different forms, as we discuss next.

### 2.2.1 Real spherical harmonics

We expand the eigensolutions of a spherically symmetric Earth model in terms of real spherical harmonics, as defined by Dahlen & Tromp (1998), such that  $\mathbf{s}_s = \mathbf{s}_s^*$ . Using real spherical harmonics in the matrix elements eqs (15)–(17), we find that the transposed matrices  $\mathbf{T}^T$ ,  $\mathbf{W}^T$  and  $\mathbf{V}^T(\nu)$  are given by

$$\mathbf{T}^T = \mathbf{T}, \quad (21)$$

$$\mathbf{W}^T = -\mathbf{W}, \quad (22)$$

$$\mathbf{V}^T(\nu) = \mathbf{V}(\nu). \quad (23)$$

Thus,  $\mathbf{T}$  and  $\mathbf{V}(\nu)$  are symmetric matrices whereas  $\mathbf{W}$  is antisymmetric. Upon taking the transpose of left eigenvalue problem eq. (19), we find the auxiliary right eigenvalue problem (Dahlen & Tromp 1998, eq. 7.87)

$$[\mathbf{V}(\nu) - 2\nu \mathbf{W} - \nu^2 \mathbf{T}] \bar{\mathbf{q}} = \mathbf{0}. \quad (24)$$

This right eigenvalue problem may be used to find the left eigensolutions  $\bar{\mathbf{q}}$  of eq. (19). Note that this eigenvalue problem may be obtained from the right eigenvalue problem eq. (20) by changing the sense of the Earth's rotation.

For practical and historical reasons, expressions for matrix elements in the literature (e.g. Woodhouse & Dahlen 1978; Woodhouse 1980; Mochizuki 1986; Tanimoto 1986; Henson 1989; Shibata *et al.* 1991) are all in terms of complex spherical harmonics. The complex-to-real matrix transformations in appendix D. 3.3 of Dahlen & Tromp (1998) may be used to obtain real matrix elements from complex elements.

### 2.2.2 Complex spherical harmonics

Next, let us expand the eigensolutions of a spherically symmetric Earth model,  $\mathbf{s}_s$ , in terms of complex spherical harmonics, as defined by Woodhouse (1980). Using the relations (4)–(6) and the symmetry eq. (2), we find that the Hermitian transposed matrices  $\mathbf{T}^H$ ,  $\mathbf{W}^H$  and  $\mathbf{V}^H(\nu)$  are given by

$$\mathbf{T}^H = \mathbf{T}, \quad (25)$$

$$\mathbf{W}^H = \mathbf{W}, \quad (26)$$

$$\mathbf{V}^H(\nu) = \mathbf{V}(-\nu^*). \quad (27)$$

Thus,  $\mathbf{T}$  and  $\mathbf{W}$  are Hermitian matrices while  $\mathbf{V}$  is not.

Upon taking the Hermitian transpose of left eigenvalue problem eq. (19), we find the auxiliary right eigenvalue problem

$$[\mathbf{V}(-v^*) - 2(-v^*)\mathbf{W} - (-v^*)^2\mathbf{T}]\bar{\mathbf{q}}^* = \mathbf{0}. \quad (28)$$

This right eigenvalue problem yields eigensolutions  $\bar{\mathbf{q}}^*$  with associated eigenvalues  $-v^*$ , and thus the sought left eigensolutions  $\bar{\mathbf{q}}$  of eq. (19) may be obtained by taking the complex conjugates of  $\bar{\mathbf{q}}^*$ . Unlike the auxiliary right eigenvalue problem in terms of real spherical harmonics eq. (24), eq. (28) is not simply obtained by reversing the Earth's sense of rotation in the original right eigenvalue problem eq. (20).

### 2.3 Anelasticity

Anelasticity may be accounted for by introducing physical dispersion and intrinsic attenuation, leading to a frequency-dependent coupling matrix  $\mathbf{V}$ . For example, in an isotropic absorption-band Earth model the bulk and shear moduli take the form (see Dahlen & Tromp 1998, section 6.1)

$$\kappa \longrightarrow \kappa_r \left[ 1 + \frac{2}{\pi Q_\kappa} \ln(|\omega/\omega_r|) + i \operatorname{sgn}(\omega) Q_\kappa^{-1} \right], \quad (29)$$

$$\mu \longrightarrow \mu_r \left[ 1 + \frac{2}{\pi Q_\mu} \ln(|\omega/\omega_r|) + i \operatorname{sgn}(\omega) Q_\mu^{-1} \right], \quad (30)$$

where a subscript  $r$  denotes the modulus at (positive) reference frequency  $\omega_r$ , and  $Q_\kappa$  and  $Q_\mu$  denote the intrinsic bulk and shear quality factors, which are nearly frequency-independent within the normal-mode frequency band (Kanamori & Anderson 1977).

For a constant- $Q$  absorption-band model, the coupling matrix  $\mathbf{V}$  may be broken down as follows:

$$\mathbf{V}(v) = \mathbf{V}_0 + \mathbf{V}^{\text{cen}} + \mathbf{V}^{\text{ell+lat}}(\omega) + i \mathbf{A}^{\text{lat}}, \quad \omega > 0, \quad (31)$$

where  $\mathbf{V}_0$  is a diagonal matrix with the squared spherical anelastic Earth reference eigenfrequencies on its diagonal,  $\mathbf{V}^{\text{cen}}$  denotes contributions due to the centrifugal potential,  $\mathbf{V}^{\text{ell+lat}}$  denotes contribution due to ellipticity and other types of lateral heterogeneity and  $\mathbf{A}^{\text{lat}}$  denotes contributions due to lateral variations in intrinsic attenuation. The reference frequencies of the spherical Earth model may include spherically symmetric attenuation in which case these reference eigenfrequencies are complex. Explicit expressions for the various contributions are documented in appendix D.2 of Dahlen & Tromp (1998). The challenge is to accommodate the frequency dependence of the moduli in the construction of  $\mathbf{V}(v)$ , which comes via the logarithmic physical dispersion terms in the expressions for the moduli eqs (29) and (30). This frequency dependence only affects the contribution  $\mathbf{V}^{\text{ell+lat}}$ .

In order to take anelasticity into account and make solving the eigenvalue problems eqs (19) and (20) tractable, two approaches are proposed. First, since the perturbed Earth deviates only slightly from the unperturbed Earth, we may approximate  $\mathbf{V}(v)$  by  $\mathbf{V}(v_f)$  as in Deuss & Woodhouse (2001), where the fiducial frequency  $v_f$  is a geometric average over the degenerate frequencies of two coupled modes, that is

$$v_f = \sqrt{v_s v_{s'}}. \quad (32)$$

This assumption leads to the quadratic left and right eigenvalue problems

$$\bar{\mathbf{q}}^T [\mathbf{V}(v_f) + 2v\mathbf{W} - v^2\mathbf{T}] = \mathbf{0}, \quad (33)$$

$$[\mathbf{V}(v_f) + 2v\mathbf{W} - v^2\mathbf{T}]\mathbf{q} = \mathbf{0}, \quad (34)$$

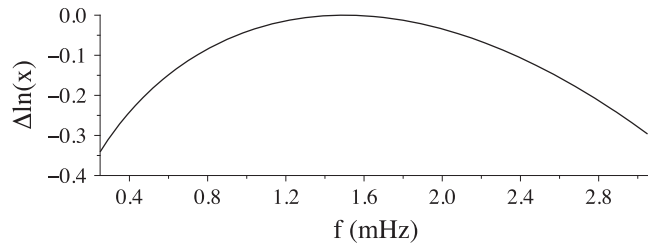


**Figure 1.** Accuracy of the quadratic approximation of logarithmic physical dispersion based on eq. (38). Relative difference  $\Delta \ln(x) = [-\frac{3}{2} + 2x - \frac{1}{2}x^2 - \ln(x)]/\ln(x)$ , where  $x = |\omega/\omega_r|$ , using a reference frequency  $\omega_r$  of 1.5 mHz, corresponding to the centre of the frequency band of interest. Near the edges of the band, the difference between the logarithmic physical dispersion term and its second-order accurate approximation eq. (38) can be 30 per cent.

respectively. In real spherical harmonics, the left eigenvalue problem eq. (33) may be replaced by the right eigenvalue problem

$$[\mathbf{V}(v_f) - 2v\mathbf{W} - v^2\mathbf{T}]\bar{\mathbf{q}} = \mathbf{0}. \quad (35)$$

In complex spherical harmonics, we have instead

$$[\mathbf{V}^H(v_f) - 2(-v^*)\mathbf{W} - (-v^*)^2\mathbf{T}]\bar{\mathbf{q}}^* = \mathbf{0}. \quad (36)$$

The normalization eq. (18) becomes

$$\bar{\mathbf{q}}^T [\mathbf{T} - v^{-1}\mathbf{W} - \frac{1}{2}v^{-1}\partial_v \mathbf{V}(v_f)]\mathbf{q} = 1. \quad (37)$$

Alternatively, the second approach is to carry out a Taylor expansion of the logarithmic dispersion term up to second-order around  $\omega_r$  (Park & Gilbert 1986):

$$\ln(|\omega/\omega_r|) \sim a + b|\omega| + c\omega^2, \quad (38)$$

where  $a = -3/2$ ,  $b = 2\omega_r^{-1}$  and  $c = -\frac{1}{2}\omega_r^{-2}$  with  $\omega_r > 0$ . Fig. 1 illustrates that the quadratic approximation eq. (38) is acceptable over the normal-mode frequency range from 0.3 to 3 mHz. Thus, we take physical dispersion into account based on the quadratic approximation eq. (38), using a reference frequency of 1.5 mHz, corresponding to the centre of the frequency band of interest. This approach also leads to quadratic left and right eigenvalue problems, namely

$$\bar{\mathbf{q}}^T (\mathbf{K} + v\mathbf{C} + v^2\mathbf{M}) = \mathbf{0}, \quad (39)$$

$$(\mathbf{K} + v\mathbf{C} + v^2\mathbf{M})\mathbf{q} = \mathbf{0}, \quad (40)$$

where

$$\mathbf{K} = \mathbf{V}_0 + \mathbf{V}^{\text{cen}} + \mathbf{V}_{\text{ref}}^{\text{ell+lat}} + a\mathbf{V}_{\text{pd}}^{\text{ell+lat}} + i\mathbf{A}^{\text{lat}}, \quad (41)$$

$$\mathbf{C} = 2\mathbf{W} + b\mathbf{V}_{\text{pd}}^{\text{ell+lat}}, \quad (42)$$

$$\mathbf{M} = -\mathbf{T} + c\mathbf{V}_{\text{pd}}^{\text{ell+lat}}. \quad (43)$$

The matrix elements  $\mathbf{V}^{\text{ell+lat}}$  have been split in terms a contribution at the reference frequency  $\omega_r$ ,  $\mathbf{V}_{\text{ref}}^{\text{ell+lat}}$ , plus a term that multiplies the logarithmic physical dispersion  $\ln(|\omega/\omega_r|)$ ,  $\mathbf{V}_{\text{pd}}^{\text{ell+lat}}$ . In real spherical harmonics, the left eigenvalue problem eq. (39) may be replaced by the right eigenvalue problem via eq. (24)

$$(\mathbf{K} - v\mathbf{C}' + v^2\mathbf{M})\bar{\mathbf{q}} = \mathbf{0}, \quad (44)$$

where

$$\mathbf{C}' = 2\mathbf{W} - b\mathbf{V}_{\text{pd}}^{\text{ell+lat}}. \quad (45)$$

In complex spherical harmonics, we have instead

$$[\mathbf{K}' - (-\nu^*)\mathbf{C} + (-\nu^*)^2\mathbf{M}]\bar{\mathbf{q}}^* = \mathbf{0}, \quad (46)$$

where

$$\mathbf{K}' = \mathbf{V}_0^* + \mathbf{V}^{\text{cen}} + \mathbf{V}_{\text{ref}}^{\text{ell+lat}} + a\mathbf{V}_{\text{pd}}^{\text{ell+lat}} - i\mathbf{A}^{\text{lat}}. \quad (47)$$

Finally, the normalization eq. (18) becomes

$$\bar{\mathbf{q}}^T(-\mathbf{M} - \frac{1}{2}\nu^{-1}\mathbf{C})\mathbf{q} = 1. \quad (48)$$

## 2.4 Synthetic seismograms: wideband coupling

The time-domain displacement,  $\mathbf{s}$ , due to a distributed body force,  $\mathbf{f}$ , may be expressed in terms of the Green's tensor,  $\mathbf{G}$ , as

$$\mathbf{s}(\mathbf{x}_r, t) = \int_{-\infty}^t \int_{V_s} \mathbf{G}(\mathbf{x}_r, \mathbf{x}_s; t - t_s) \cdot \mathbf{f}(t_s, \mathbf{x}_s) dV_s dt_s, \quad (49)$$

where  $\mathbf{x}_r$  denotes a receiver location. Let us use an index  $k$  to label the eigensolutions  $\mathbf{s}_k$  with associated eigenfrequencies  $\nu_k$ . The eigensolutions of the anti-Earth are similarly identified as  $\bar{\mathbf{s}}_k$  with the same eigenfrequency  $\nu_k$  (see Table 1). The Green's tensor may be expressed in terms of these eigensolutions as (see section 6.3.3 of Dahlen & Tromp 1998)

$$\mathbf{G}(\mathbf{x}_r, \mathbf{x}_s; t) = \text{Re} \sum_k (i\nu_k)^{-1} \mathbf{s}_k(\mathbf{x}_r) \bar{\mathbf{s}}_k(\mathbf{x}_s) e^{i\nu_k t}. \quad (50)$$

The acceleration response to a step-function moment-tensor source may be conveniently expressed in terms of spherical Earth receiver and source vectors

$$\mathbf{r} = \begin{pmatrix} \vdots \\ \hat{\nu} \cdot \mathbf{s}_s(\mathbf{x}_r) \\ \vdots \end{pmatrix}, \quad (51)$$

$$\mathbf{s} = \begin{pmatrix} \vdots \\ \mathbf{M} : \boldsymbol{\epsilon}_s^*(\mathbf{x}_s) \\ \vdots \end{pmatrix}, \quad (52)$$

where  $\hat{\nu}$  denotes the polarization of the accelerometer,  $\mathbf{M}$  denotes the moment tensor (Saito 1967; Gilbert 1970) and

$$\boldsymbol{\epsilon}_s = \frac{1}{2} [\nabla \mathbf{s}_s + (\nabla \mathbf{s}_s)^T] \quad (53)$$

is the strain associated with the spherical eigensolution  $\mathbf{s}_s$ . If the spherically symmetric eigensolutions are expanded in real spherical harmonics  $\boldsymbol{\epsilon}_s^* = \boldsymbol{\epsilon}_s$  and the source vector  $\mathbf{s}$  is real, but the representation eq. (52) keeps our options open.

The  $\hat{\nu}$  component of acceleration is

$$a(t) = \hat{\nu} \cdot \partial_t^2 \mathbf{s}(\mathbf{x}_r, t). \quad (54)$$

Using the receiver and source vectors (eqs 51 and 52), this accelerogram may be expressed algebraically as

$$a(t) = \text{Re} [\mathbf{r}'^T \exp(i\mathbf{N}t) \mathbf{s}'], \quad (55)$$

where we have introduced the transformed receiver and source vectors

$$\mathbf{r}' = \mathbf{Q}^T \mathbf{r}, \quad (56)$$

$$\mathbf{s}' = \bar{\mathbf{Q}}^T \mathbf{s}. \quad (57)$$

The diagonal matrix  $\mathbf{N}$  contains the eigenfrequencies  $\nu_k$ , and the matrices  $\mathbf{Q}$  and  $\bar{\mathbf{Q}}$  have the eigensolutions  $\mathbf{q}_k$  and  $\bar{\mathbf{q}}_k$  associated with eigenfrequency  $\nu_k$  as their respective columns. In this notation, relationship eq. (11) may be rewritten as

$$\mathbf{s}_k = \sum_s Q_{sk} \mathbf{s}_s, \quad (58)$$

with anti-Earth complement

$$\bar{\mathbf{s}}_k = \sum_s \bar{Q}_{sk} \mathbf{s}_s. \quad (59)$$

The accelerogram eq. (55) is valid for a general 3-D Earth model and may be used to calculate broad-band synthetic spectra. We refer to this approach as ‘wideband’ coupling.

## 2.5 Quasi-degenerate perturbation theory: reduction to group and self-coupling

Solving left and right quadratic eigenvalue problems is computationally expensive. To reduce the computational expense, we can focus on groups of relatively isolated modes in the free oscillation spectrum while at the same time linearizing the eigenvalue problem. By linearizing the frequency perturbations around a suitably chosen fiducial frequency  $\omega_r$ , the eigenvalue problems can be reduced to standard linear eigenvalue problems for which many numerical routines are valuable (e.g. LAPACK). In the isolated-mode approximation, only self-coupling of the singlets within the same multiplet is considered.

Ignoring terms higher than first order in  $\delta\nu = \nu - \omega_r$ ,  $\mathbf{V}$ ,  $\mathbf{W}$  and  $\mathbf{T}$ , we make the approximation

$$\mathbf{V}(\nu) + 2\nu \mathbf{W} - \nu^2 \mathbf{T} \approx 2\omega_r (\mathbf{H} - \delta\nu \mathbf{I}), \quad (60)$$

where

$$\mathbf{H} = \mathbf{N}_0 - \omega_r \mathbf{I} + \mathbf{W} + (2\omega_r)^{-1} (\mathbf{V}' + i\mathbf{A}^{\text{lat}} - \omega_r^2 \mathbf{T}'). \quad (61)$$

Here  $\mathbf{N}_0$  is a diagonal matrix composed of the unperturbed eigenfrequencies  $\nu_s$ ,  $\mathbf{I}$  is the identity matrix, and

$$\mathbf{V}' = \mathbf{V}^{\text{cen}} + \mathbf{V}_{\text{ref}}^{\text{ell+lat}}, \quad (62)$$

$$\mathbf{T}' = \mathbf{T} - \mathbf{I}. \quad (63)$$

How we proceed depends on the choice of real versus complex spherical harmonics.

### 2.5.1 Real spherical harmonics

In this section—where we use real spherical harmonics such that  $\mathbf{s}_s^* = \mathbf{s}_s$ —we recapitulate results in Chapter 13.2 of Dahlen & Tromp (1998). We consider the two standard linear eigenvalue problems

$$\mathbf{H} \mathbf{z} = \delta\nu \mathbf{z}, \quad (64)$$

$$\bar{\mathbf{H}} \bar{\mathbf{z}} = \delta\nu \bar{\mathbf{z}}, \quad (65)$$

where

$$\bar{\mathbf{H}} = \mathbf{N}_0 - \omega_r \mathbf{I} - \mathbf{W} + (2\omega_r)^{-1} (\mathbf{V}' + i\mathbf{A}^{\text{lat}} - \omega_r^2 \mathbf{T}'). \quad (66)$$

The second standard eigenvalue problem is a linearized version of eq. (24). Upon taking the transpose of the right eigenvalue problem eq. (65) and using the fact that  $\bar{\mathbf{H}} = \mathbf{H}^T$ , we find that

$$\bar{\mathbf{z}}^T \mathbf{H} = \delta\nu \bar{\mathbf{z}}^T, \quad (67)$$

and thus we recognize  $\bar{\mathbf{z}}$  as the left eigensolution of  $\mathbf{H}$ . We normalize the left and right eigensolutions such that

$$\bar{\mathbf{z}}^T \mathbf{z} = 1. \quad (68)$$

The question is how the eigensolution pairs  $\mathbf{z}$ ,  $\bar{\mathbf{z}}$  and  $\mathbf{q}$ ,  $\bar{\mathbf{q}}$  are related.

Let us consider the normalization of the eigensolution pair  $\mathbf{q}$ ,  $\bar{\mathbf{q}}$  expressed by eq. (18). By inserting eq. (31) into eq. (18) and ignoring the contribution of ellipticity to  $\partial_v \mathbf{V}(v)$ , we may expand  $\mathbf{I} + \mathbf{T}' - v^{-1} \mathbf{W} - \frac{1}{2} v^{-1} \partial_v \mathbf{V}(v)$  up to first order around  $\omega_r$  so that eq. (18) becomes

$$\bar{\mathbf{q}}^T \mathbf{B}^{-2} \mathbf{q} = 1, \quad (69)$$

where

$$\mathbf{B} = \mathbf{I} - \frac{1}{2} \mathbf{T}' + \frac{\omega_r^{-2}}{2\pi} \mathbf{A}^{\text{lat}} + \frac{\omega_r^{-1}}{2} \mathbf{W}. \quad (70)$$

Note that the third term on the right-hand side of eq. (70) is due to anelastic dispersion, rather than anelastic attenuation. Upon comparing the normalization eqs (68) and (69), we conclude that eigensolution pairs  $\mathbf{z}$ ,  $\bar{\mathbf{z}}$  and  $\mathbf{q}$ ,  $\bar{\mathbf{q}}$  are related via

$$\mathbf{q} = \mathbf{B} \mathbf{z}, \quad (71)$$

$$\bar{\mathbf{q}} = \mathbf{B}^T \bar{\mathbf{z}}. \quad (72)$$

The acceleration is of the form eq. (55), namely,

$$a(t) = \text{Re} [\mathbf{r}'^T \exp(i\mathbf{N}t) \mathbf{s}'], \quad (73)$$

but in this case the diagonal matrix  $\mathbf{N}$  contains the perturbed eigenfrequencies,  $\nu_k = \omega_r + \delta\nu_k$ , of the singlets in the group, and the receiver and source vectors are

$$\mathbf{r}' = \mathbf{Q}^T \mathbf{r} = \mathbf{Z}^T \mathbf{B}^T \mathbf{r} \quad (74)$$

$$\mathbf{s}' = \bar{\mathbf{Q}}^T \mathbf{s} = \bar{\mathbf{Z}}^T \mathbf{B} \mathbf{s}. \quad (75)$$

where the matrices  $\mathbf{Z}$  and  $\bar{\mathbf{Z}}$  have the eigensolutions  $\mathbf{z}_k$  and  $\bar{\mathbf{z}}_k$  as their respective columns. The acceleration may now be expressed in the form

$$a(t) = \text{Re} [(\mathbf{Z}^T \mathbf{B}^T \mathbf{r})^T \exp(i\mathbf{N}t) (\bar{\mathbf{Z}}^T \mathbf{B} \mathbf{s})]. \quad (76)$$

### 2.5.2 Complex spherical harmonics

In the case of complex spherical harmonics, we consider the standard linear eigenvalue problems

$$\mathbf{H} \mathbf{z} = \delta\nu \mathbf{z}, \quad (77)$$

$$\bar{\mathbf{H}} \bar{\mathbf{z}} = (\delta\nu)^* \bar{\mathbf{z}}, \quad (78)$$

where

$$\bar{\mathbf{H}} = \mathbf{N}_0^* - \omega_r \mathbf{I} + \mathbf{W} + (2\omega_r)^{-1} (\mathbf{V}' - i \mathbf{A}^{\text{lat}} - \omega_r^2 \mathbf{T}'), \quad (79)$$

and

$$(\delta\nu)^* = \nu^* - \omega_r. \quad (80)$$

Likewise, the second standard eigenvalue problem is a linearized version of eq. (28). Upon taking the Hermitian transpose of the right eigenvalue problem eq. (78) and using the fact that  $\bar{\mathbf{H}} = \mathbf{H}^H$ , we find that

$$\bar{\mathbf{z}}^H \mathbf{H} = \delta\nu \bar{\mathbf{z}}^H, \quad (81)$$

and thus we recognize  $\bar{\mathbf{z}}$  as the left eigensolution of  $\mathbf{H}$ . We normalize the left and right eigensolutions such that

$$\bar{\mathbf{z}}^H \mathbf{z} = 1. \quad (82)$$

The linearized normalization condition for the eigensolutions  $\mathbf{q}$  and  $\bar{\mathbf{q}}$  remains (eq. 69), where in the case of complex spherical harmonics the matrix  $\mathbf{B}$  is Hermitian:  $\mathbf{B} = \mathbf{B}^H$ . Thus, we find that in this case

$$\mathbf{q} = \mathbf{B} \mathbf{z}, \quad (83)$$

$$\bar{\mathbf{q}} = \mathbf{B}^T \bar{\mathbf{z}}^*. \quad (84)$$

The acceleration is of the form eq. (73), but the receiver and source vectors are

$$\mathbf{r}' = \mathbf{Q}^T \mathbf{r} = \mathbf{Z}^T \mathbf{B}^T \mathbf{r} = (\mathbf{Z}^H \mathbf{B}^H \mathbf{r}^*)^* = (\mathbf{Z}^H \mathbf{B} \mathbf{r}^*)^* \quad (85)$$

$$\mathbf{s}' = \bar{\mathbf{Q}}^T \mathbf{s} = \bar{\mathbf{Z}}^H \mathbf{B} \mathbf{s}, \quad (86)$$

where the matrices  $\mathbf{Z}$  and  $\bar{\mathbf{Z}}$  have the eigensolutions  $\mathbf{z}_k$  and  $\bar{\mathbf{z}}_k$  as their respective columns. The acceleration may now be expressed in the form

$$a(t) = \text{Re} [(\mathbf{Z}^H \mathbf{B} \mathbf{r}^*)^H \exp(i\mathbf{N}t) (\bar{\mathbf{Z}}^H \mathbf{B} \mathbf{s})]. \quad (87)$$

Alternatively, one may derive eigensolutions in terms of complex spherical harmonics from those expressed in real spherical harmonics by invoking a transformation matrix (see appendix D.3.3 of Dahlen & Tromp 1998).

Besides accelerating the calculations, the reduction to a standard linear eigenvalue problem results in the simultaneous determination of left and right eigenvectors. We can thus simply replace  $\bar{\mathbf{Z}}^T$  in eq. (76) and  $\bar{\mathbf{Z}}^H$  in eq. (87) with  $\mathbf{Z}^{-1}$ .

## 3 NUMERICAL EXAMPLES

In the previous section, we discussed the calculation of synthetic seismograms on a rotating, anelastic Earth model based on perturbation theory and quasi-degenerate perturbation theory. In this section, we implement these theoretical results in practice, with an emphasis on assessing the accuracy of various commonly used approximations. In addition to re-evaluating the narrowband- and self-coupling approximations against wideband coupling in a systematic manner, we investigate issues related to physical dispersion and (re)normalization. Spectra employing approximate frequency and coupling matrices, which lead to a linearized eigenvalue problem, are also examined.

We use 3-D shear wave speed model S20RTS (Ritsema *et al.* 1999), which uses PREM (Dziewonski & Anderson 1981) plus anelastic model of QL6 (Durek & Ekström 1996) as the terrestrial monopole. Perturbations in bulk modulus and density are scaled from the shear modulus by factors of 0.5 and 0.4, respectively. Moho variations are taken from crustal model Crust 1.0 (Laske *et al.* 2013), and we accommodate rotation and ellipticity. We do not consider lateral variations in attenuation, although these may be important (Millot-Langet *et al.* 2003) and can be readily accommodated.

Degenerate eigenfrequencies of the anelastic terrestrial monopole may be calculated from the chosen spherical Earth model (i.e. PREM plus QL6), but we use centre frequencies and quality factors from the Reference Earth Model website compiled by G. Laske ([igppweb.ucsd.edu/~gabi/rem.html](http://igppweb.ucsd.edu/~gabi/rem.html)). It is common practice in free oscillation seismology—particularly in tomographic studies

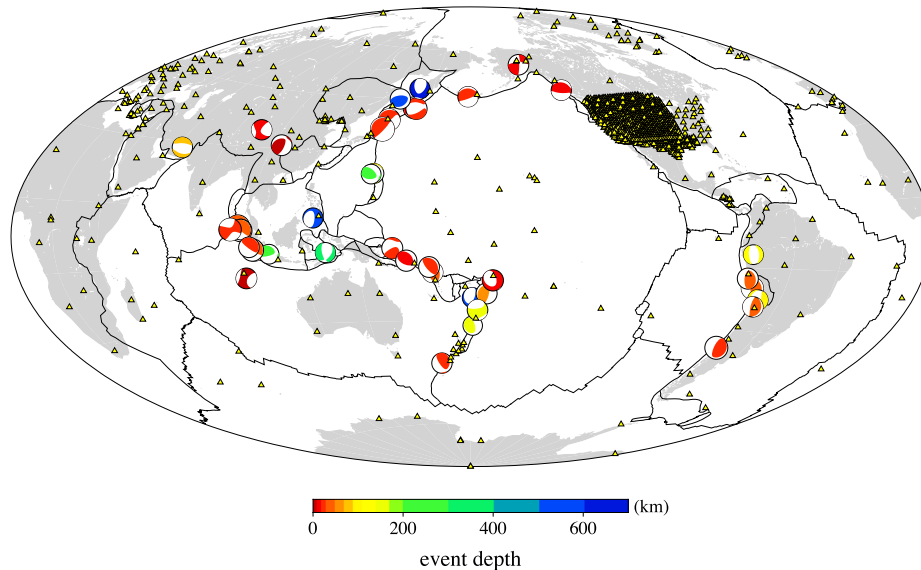


**Figure 2.** Map showing the stations (yellow triangles) and locations and mechanisms of 41 earthquakes used in this study (beach balls).

where the focus is on lateral variations—to change centre frequencies from model predictions to their observed values. This amounts to recognizing that none of the current 1-D Earth models are perfect terrestrial monopoles, thereby also circumventing a debate about the choice of 1-D model. Spectral differences between data and synthetics may significantly change due to centre–frequency shifts, but it is immaterial for comparisons of synthetics.

We calculate more than 10 000 synthetic spectra for 41 earthquakes with  $M_w > 7.8$  occurring between 2000 and 2013 (Fig. 2). We focus on 116 multiplets—a total of 1880 singlets—with frequencies below 3 mHz. We use SLEPc (`slep.c.upv.es`; Hernandez *et al.* 2005) to solve eigenvalue problems, including (1) quadratic eigenvalue problems for the wideband- and narrowband-coupling scheme; (2) standard linear eigenvalue problems encountered in quasi-degenerate perturbation theory; (3) linear eigenvalue problems—including standard and generalized eigenvalue problems—associated with various approximations to general nonlinear eigenvalue problems.

Despite the availability of nonlinear (direct) solvers in the SLEPc library, we use a linear solver for computational efficiency. In this approach, a quadratic eigenvalue problem is first transformed into a linear generalized eigenvalue problem by doubling the size of the matrices, an approach first proposed in geophysics by Wahr (1981) and subsequently used by Master *et al.* (1983), Park & Gilbert (1986) and Deuss & Woodhouse (2001). The linear system is preconditioned by the block Jacobi technique (e.g. Saad 2003), and solved based on the Krylov–Schur subspace iterative method (Stewart 2001) with the Generalized Minimal Residual (GMRES) algorithm (Saad & Schultz 1986). It requires 41 iterations to reach relative residual errors smaller than  $10^{-12}$ . The numerical cost is  $\sim 4.3$  hr on a single processor of a quad core Intel Xeon 2.4 GHz CPU for two eigenproblems (i.e. the original and auxiliary problems) with an upper-limit frequency of 3 mHz. The compute time roughly scales with the sixth power of the upper-limit frequency of the system (see Fig. 3), which is one order less than the approach of Al-Attar *et al.* (2012). In addition to the GMRES algorithm, we also used the Bi-Conjugate Gradient Squared (BCGS) algorithm (van der Vorst 1992), which is employed by Al-Attar *et al.* (2012). Both algorithms show similar patterns for compute time and scalability for the Earth’s free-oscillation system.

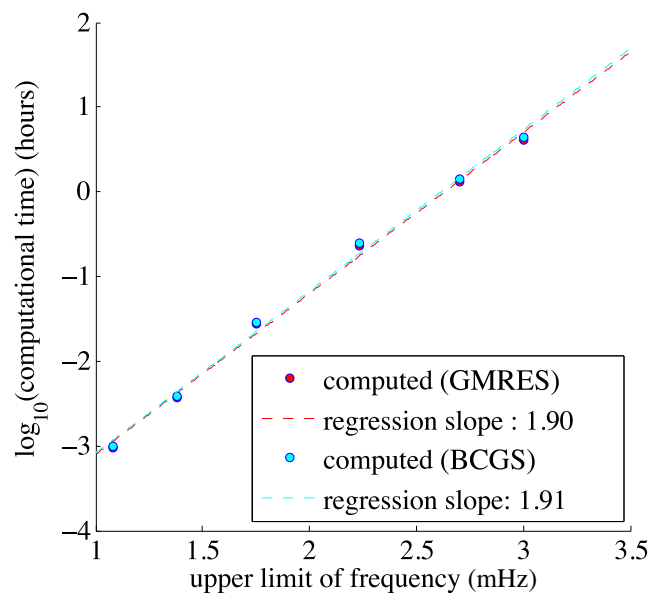


**Figure 3.** Compute times for quadratic eigenvalue problems with different upper-limit frequencies (i.e. different matrix sizes). Two iterative algorithms, namely, GMRES (red) and BCGS (cyan), are used for comparison. The compute times for both approaches basically coincide. Dashed lines represent linear regressions with slopes of 1.90 and 1.91 for the two algorithms, respectively. These results indicate that the calculations roughly scale as  $\omega^6$ .

To begin with, we address the importance of the balance between computational efficiency and accuracy in the construction of coupling matrices, prior to invoking the SLEPc solver. We find that radial integrations are the most time-consuming part ( $\sim 80$  per cent) of the matrix calculations, and variations in knot spacing can significantly affect their accuracy. With this concern in mind, we calculated three normal-mode catalogues for the terrestrial monopole using two unevenly spaced radial grids with 808 and 1602 knots, and one evenly spaced radial grid with 6386 integration points based on the open-source mode calculation package MINEOS (`geodynamics.org`). Although the eigensolutions—of the perturbed Earth model—for these three cases are virtually indistinguishable, resulting normal-mode spectra can differ considerably,

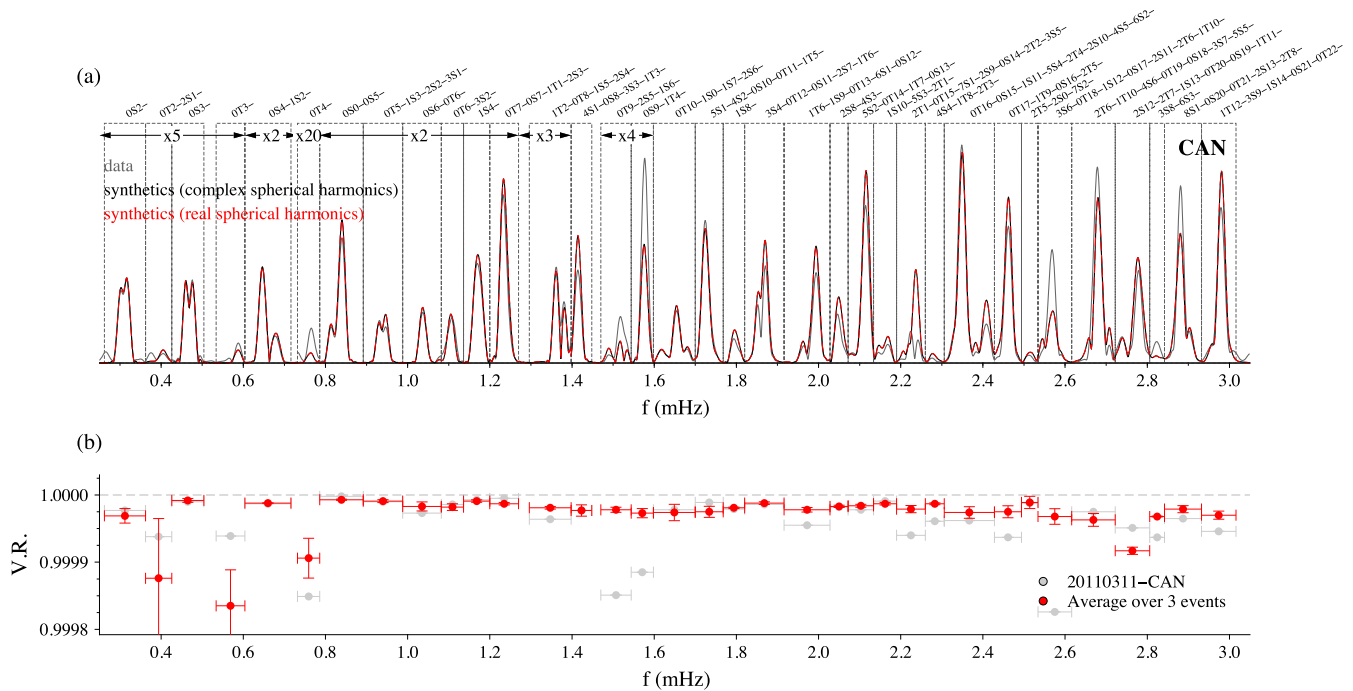


**Figure 4.** Wideband coupling in real and complex spherical harmonic bases. (a) Vertical-component acceleration amplitude spectra at station CAN (Canberra, Australia) for the 2011 Tohoku earthquake. A Hanning taper is applied to a 6–36 hr time window relative to the centroid time. Synthetics are calculated based on wideband coupling all modes below 3 mHz in real (red curve) and complex (black curve) spherical harmonic bases. Data are depicted by the grey curve. The number at the centre of the black horizontal arrows labels the factor by which the vertical axis is exaggerated within the frequency window spanned by the arrow. We divided the spectrum into several target frequency windows (dashed rectangles) in which prominent modes (labelled along the top) are identified by their degenerate eigenfrequencies. (b) Using the synthetics based on complex spherical harmonics as a reference, the difference with the synthetics based on real spherical harmonics is calculated using eq. (88). Perfect agreement corresponds to a variance reduction (V.R.) of 1.0. The grey symbols denote the difference for the synthetics shown in (a), whereas the red symbols show an average over three depth-distinct events. In either case, the level of agreement (a difference of <0.02 per cent) is excellent.

in particular at higher frequencies. The differences do not show a trend, that is, 1602-knot simulations are not closer to 6386-knot simulations than 808-knot simulations. The cause of these differences is proper eigensolution normalization. Instead of using the eigensolutions as provided by the eigenvalue solver, we impose normalization based on eq. (68) and find that in that case all three catalogues produce identical spectra. Based on these experiments we selected a mode catalogue with 1602 radial knots. As a further check of the reliability of the eigensolutions, we compare  $\mathbf{H}\mathbf{z}$  with  $\mathbf{z}v$  (Roman *et al.* 2014) and find that the relative residual errors for all modes are smaller than  $10^{-12}$ . In addition, we have no trouble pairing the eigenvalues of the original (left) eigenproblem with those of the auxiliary (right) eigenproblem because the two corresponding eigenvalues are numerically indistinguishable up to double precision even quadratic problems with  $1880 \times 1880$  matrices.

To assess the quality of various approximations, we compare a complex spectrum of interest,  $a_{i,j}$ , to a reference spectrum,  $a_{i,j}^{\text{ref}}$ —usually an ‘exact’ spectrum calculated based on wideband coupling below 3 mHz using eq. (55)—by calculating the variance reduction

$$\text{V.R.} = 1 - \sqrt{\frac{\sum_{i=1}^{\text{nevt}} \sum_{j=1}^{\text{nstn}} w_i w_j (a_{i,j} - a_{i,j}^{\text{ref}})^2}{\sum_{i=1}^{\text{nevt}} \sum_{j=1}^{\text{nstn}} w_i w_j (a_{i,j}^{\text{ref}})^2}}. \quad (88)$$

This represents a weighted average over stations and events in which  $w_i w_j$  is a weight determined by the spatial coverage of event  $i$  and station  $j$ .

It is noteworthy that synthetic spectra become inaccurate near the upper frequency limit, because coupling with higher-frequency modes beyond this limit is ignored. As a guide, Al-Attar *et al.* (2012) found that coupling all modes below 4.3 mHz yields accurate spectra below 3 mHz.

### 3.1 Wideband coupling in real versus complex spherical harmonics

We assess the accuracy of the ‘exact’ synthetics by comparing results based on real spherical harmonics with those based on complex spherical harmonics. In either approach, we need to solve two quadratic right eigenvalue problems, namely, eqs (40) and (44) for real spherical harmonics and eqs (40) and (46) for complex spherical harmonics.

We assess the difference between the two approaches based on the variance reduction estimator eq. (88). Error bars are calculated by first determining the weighted mean variance reduction over all stations, followed by determining the weighted standard deviation among the results. Rather than taking entire spectra, which are dominated by mantle-sensitive modes, we use the automated window selection tool FLEXWIN (Maggi *et al.* 2009) to select target frequency windows using a thousand spectra. Variance reduction as a function of target window is illustrated in Fig. 4. The differences are negligible. Even for toroidal-mode-dominated windows (e.g.  ${}_0T_3$  around 0.55 mHz), where weak shear energy leaking to the vertical component could amplify numerical error, the variance reduction remains <0.02 per cent.

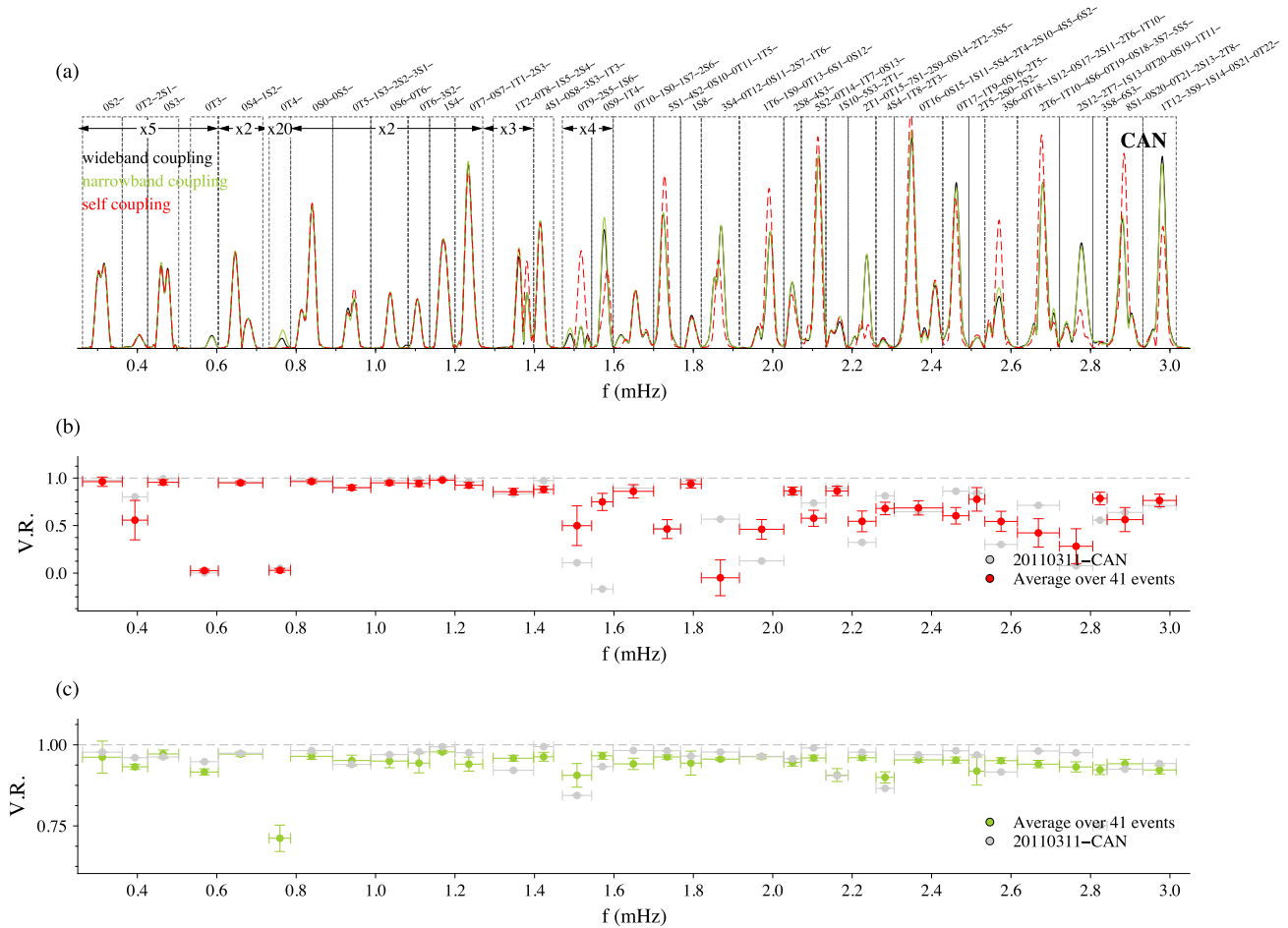


**Figure 5.** Assessment of the accuracy of narrowband- and self coupling approximations. All 116 multiplets below 3 mHz are coupled together in wideband calculations, whereas in narrowband calculations they are subdivided into the 33 supermultiplets identified by Deuss & Woodhouse (2001), and self coupling calculations consider individual contributions from the 116 multiplets. The number at the centre of the black horizontal arrows labels the factor by which the vertical axis is exaggerated within the frequency window spanned by the arrow. We divided the spectrum into frequency windows (dashed rectangles) in which prominent modes (labelled along the top) are identified by their degenerate eigenfrequencies. (a) Vertical-component acceleration amplitude spectra at station CAN (Canberra, Australia) for the 2011 Tohoku earthquake. Wideband coupling is used to calculate the ‘exact’ spectra shown in black, synthetics based on narrowband coupling are shown in green, and synthetics based on self coupling are shown in red. A Hanning taper is applied to a 6–36 hr time window relative to the centroid time. (b) Accuracy of the self coupling approximation is assessed based on eq. (88). Perfect agreement corresponds to a variance reduction (V.R.) of 1.0. Grey symbols denote the difference for the CAN synthetics shown in (a), whereas the green symbols show an average over 41 events. (c) Accuracy of the narrowband-coupling approximation is assessed based on eq. (88). Perfect agreement corresponds to a V.R. of 1.0. Grey symbols denote the difference for the CAN synthetics shown in (a), whereas the red symbols show an average over 41 events.

### 3.2 Wideband, narrowband and self coupling

In addition to grouping all modes below 3 mHz together in a wideband coupling calculation, we also consider narrowband coupling and self coupling. Comparisons among these coupling schemes were also made by Deuss & Woodhouse (2001), Andrews *et al.* (2006), Irving *et al.* (2008) and Al-Attar *et al.* (2012), and our study can be regarded as an extension of this earlier work based on a different numerical approach and a larger data set. The narrowband-coupling calculation divides the modes below 3 mHz into 33 supermultiplets, as specified by Deuss & Woodhouse (2001). The self coupling calculation considers individual contributions of all 116 modes with frequencies below 3 mHz. Spectra are calculated based on the complex spherical harmonic reference basis. Spectral differences for self coupling (Fig. 5b) and narrowband coupling (Fig. 5c) are relative to results of wideband coupling.

At frequencies below  $\sim 1.5$  mHz, except for toroidal mode windows, self coupling is acceptable, as illustrated in Fig. 5(b). This

is further corroborated by comparisons of amplitude spectra with wideband calculations (see Fig. 5a). We observe only subtle discrepancies between the two calculations (red and black curves in Fig. 5a), corresponding to very high V.R. values (grey symbols in Fig. 5b), typically larger than 0.9. The differences rapidly become unacceptable at higher frequencies. The patterns remain the same even for ensemble averages over more than 10 000 spectra (red symbols in Fig. 5b). This is to be expected because at higher frequencies the modes become denser-and-denser and across-multiplet coupling becomes more-and-more important. Note that self coupling cannot predict the occurrence of toroidal modes in vertical-component spectra (e.g.  ${}_0T_3$  and  ${}_0T_4$ ), a phenomenon that is common in observed free-oscillation spectra (Zurn *et al.* 2000). Other notable discrepancies generally involve unmodelled spheroidal-toroidal coupling (e.g. around 0.4, 1.85 and 2.75 mHz; Master *et al.* 1983), particularly for spheroidal and toroidal modes differing by one angular degree (e.g.  ${}_0S_{11-0}T_{12}$  and  ${}_0S_{19-0}T_{20}$ ), as expected based upon the angular selection rules for Coriolis coupling.

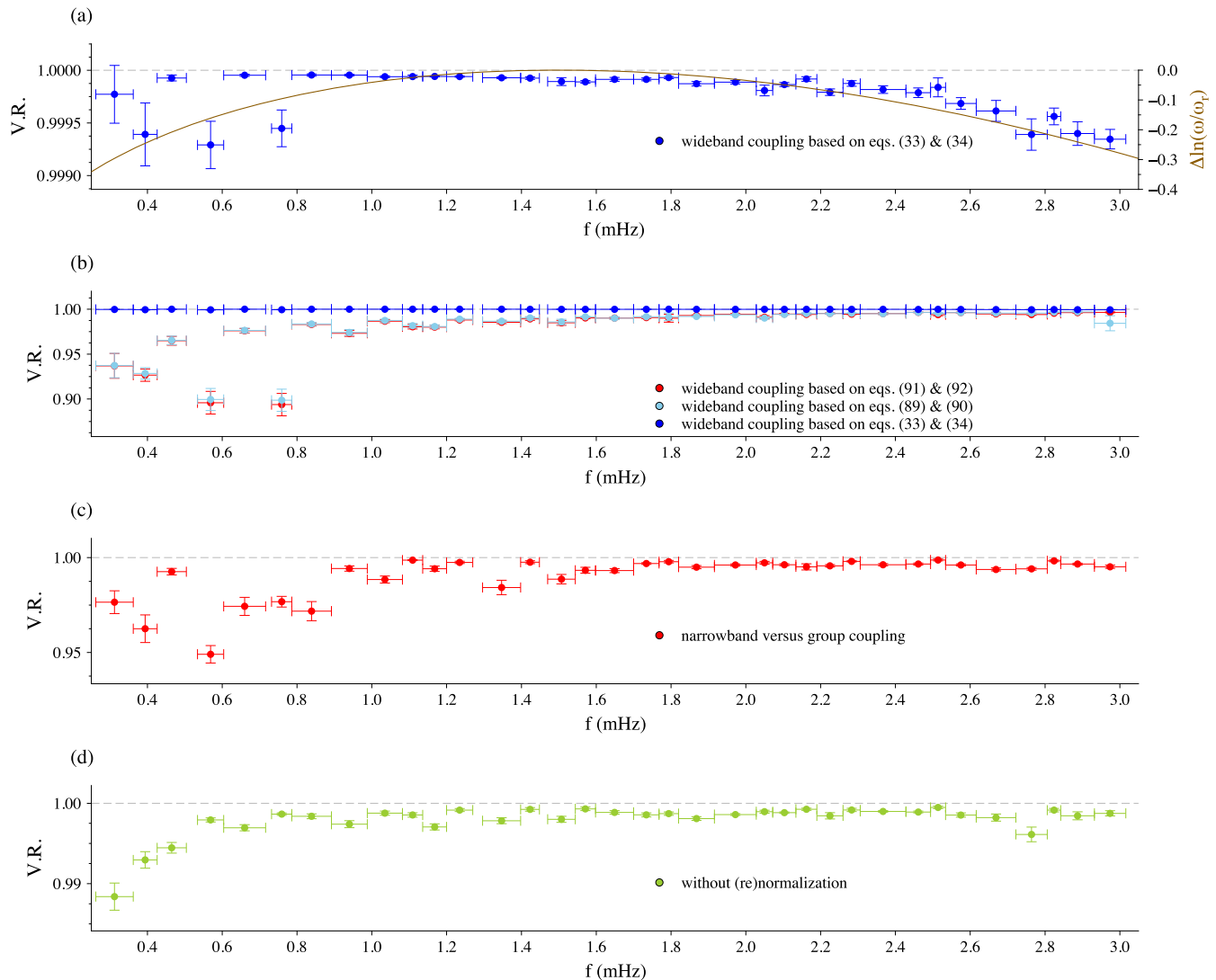


**Figure 6.** Assessment of various approximates of coupling matrices (a–c) and renormalization (d) on  $\sim 10\,000$  synthetic spectra from 41 events. (a) Comparison of spectra calculated based on (1) the fiducial frequency approximation (eq. 32) and (2) the second-order approximation of the logarithmic absorption-band dispersion effect (eq. 38). We use the latter as the reference in the variance reduction (V.R.) calculation based on eq. (88). The  $\sim 0.1$  per cent differences over the 0.3–3 mHz range are basically negligible. (b) Assessment of spectra calculated based on the fiducial frequency approximation eqs (33) and (34) involving the potential energy matrix (dark blue) with spectra calculated based on the approximation eqs (89) and (90) involving the potential energy and Coriolis matrices (light blue) and eqs (91) and (92) involving the potential energy, Coriolis and kinetic energy matrices (red). We use synthetics calculated based on the second-order approximation of the logarithmic absorption-band dispersion effect as the reference in the V.R. calculation based on eq. (88). The coupling band involves all 116 modes below 3 mHz. (c) V.R. of synthetic spectra calculated based on quasi-degenerate perturbation theory (eq. 61) relative to those obtained from the narrowband coupling scheme. Thirty-nine groups below 3 mHz are used for both calculations. (d) Comparison of wideband spectra for all modes below 3 mHz properly normalized according to eq. (18) with wideband spectra improperly normalized according to eq. (93).

Use of the narrowband approximation greatly improves the accuracy of synthetic spectra when assessed against wideband coupling, as illustrated in Fig. 5(c). Nevertheless, there is still a  $\sim 6$  per cent average misfit. Some may argue that measurement errors between synthetics and data are of the same order of magnitude as these theoretical limitations. However, we believe measurement errors are random, as opposed to systematic errors caused by the choice of coupling scheme.

The time series used in this section are Hanning tapered starting 6 hr after the centroid time and ending 30 hr thereafter. A complementary analysis using a 16–65 hr window—emphasizing longer-lasting high quality factor modes—yields similar results.

### 3.3 Effects of physical dispersion

In Section 2.3, we proposed two ways of accommodating the effects of physical dispersion on the elastic-gravitational potential energy matrix,  $\mathbf{V}(\nu)$ : (1) the fiducial frequency approximation (eq. 32, Deuss & Woodhouse 2001) and (2) the second-order approximation of the logarithmic absorption-band dispersion effect (eq. 38, Park & Gilbert 1986). Within a narrow frequency band centred on  $\omega_r$ , the latter is presumed to be a better approximation than the former because it honestly accounts for the influence of perturbed eigenfrequencies on  $\mathbf{V}(\nu)$ . Over a wider band, this approximation starts to break down, as illustrated in Fig. 1.

We compare spectra obtained based on these two approximations in Fig. 6(a), using the results from the second-order logarithmic

approximation as the reference. The discrepancies ( $\sim 0.1$  per cent) over the entire range are just slightly larger than the numerical errors illustrated in Fig. 4(b). Their change with frequency, in general, correlates with the curve  $\Delta \ln(\omega/\omega_r)$  shown in Fig. 1. Therefore we can regard spectra around  $\omega \sim \omega_r$  based on the second-order logarithmic approximation as ground truth.

We evaluate the influence of approximate physical dispersion on spectra by using different reference frequencies  $\omega_r$ . The difference,  $\Delta \ln(\omega/\omega_r)$ , around  $\omega = 3$  mHz may increase by a factor of 10 as  $\omega_r$  ranges from 1.5 to 0.65 mHz. The resulting spectral differences, however, are less than 1 per cent. Thus, despite the inexact second-order approximation of physical dispersion employed in this study, its influence on spectra is minor ( $< 1$  per cent), provided a suitable reference frequency is chosen. The simplest strategy is to evaluate self coupling contributions to the physical dispersion part of the potential energy matrix at the reference frequency of the mode in question, and cross-coupling contributions at the geometric mean frequency of the two coupled modes. Nevertheless, we are discussing tiny changes in spectra, and both treatments of physical dispersion are appropriate in the 0.3–3 mHz range.

### 3.4 Other linearization and quasi-degenerate perturbation theory

In the previous section, we approximated physical dispersion by the fiducial frequency  $\nu_f$  (eq. 32), leading quadratic left and right eigenvalue problems (eqs 33 and 34). Likewise, two popular additional approximations involve linearizing the entire eigenvalue problem around a suitably chosen fiducial frequency,  $\nu_f$ . In the first approach, only the frequency dependence of the Coriolis contribution is approximated at  $\nu_f$  (Master *et al.* 1983; Hara *et al.* 1993; Deuss & Woodhouse 2001):

$$\bar{\mathbf{q}}^T [\mathbf{V}(\nu_f) + 2\nu_f \mathbf{W} - \nu^2 \mathbf{T}] = 0, \quad (89)$$

$$[\mathbf{V}(\nu_f) + 2\nu_f \mathbf{W} - \nu^2 \mathbf{T}] \mathbf{q} = 0, \quad (90)$$

thus, leading to linear generalized eigenvalue problems in  $\nu^2$ . In the second approach, both the Coriolis and kinetic energy contributions are approximated (Deuss & Woodhouse 2001):

$$\bar{\mathbf{q}}^T [\mathbf{V}(\nu_f) + 2\nu_f \mathbf{W} - \nu_f^2 \mathbf{T}' - \nu^2 \mathbf{I}] = 0, \quad (91)$$

$$[\mathbf{V}(\nu_f) + 2\nu_f \mathbf{W} - \nu_f^2 \mathbf{T}' - \nu^2 \mathbf{I}] \mathbf{q} = 0, \quad (92)$$

where  $\mathbf{T}'$  is defined by eq. (63). It is noteworthy that the potential energy and the Coriolis effects in eqs (91) and (92) are of the same order, but the kinematic energy matrix includes a higher order term  $(\delta\nu)^2 \mathbf{I}$ , as in Deuss & Woodhouse (2001), because writing  $\nu = \nu_f + \delta\nu$  implies that  $\nu^2 = \nu_f^2 + 2\nu_f \delta\nu + (\delta\nu)^2$ .

Comparison of synthetics computed based on the linear eigenvalue problems eqs (89) and (90) and eqs (91) and (92) with synthetics based on the quadratic eigenvalue problem in the second-order logarithmic dispersion approximation (eq. 38) are shown in Fig. 6(b). Except for the toroidal-mode windows around 0.55 and 0.76 mHz, spectral discrepancies up to 6 per cent occur for the gravest modes below 1 mHz. There is no significant difference between the results based upon eqs (89) and (90) and those based upon eqs (91) and (92), indicating that the main cause of the discrepancies is due to the approximation of the Coriolis term, and therefore this approximation should be avoided, as suggested by Park & Gilbert (1986) and Al-Attar *et al.* (2012).

As discussed in Section 2.5, quasi-degenerate perturbation theory reduces the nonlinear eigenvalue problems eqs (19) and (20) to the

linear standard eigenvalue problems eqs (64) and (67). Group coupling based on this linearization is an approximation of narrowband coupling based on either eqs (33) and (34) or eqs (39) and (40). We compare the two approaches in Fig. 6(c), which is analogous to the comparison of linear (standard) and nonlinear wideband coupling illustrated in Fig. 6(b). At the lowest frequencies, the differences can be 5 per cent, but this depends on how modes are grouped. Modes below 3 mHz are divided into 39 groups in this calculation (Fig. 6c), different from the 33 groups used in the calculation shown in Fig. 5(c). If the three groups  ${}_0S_2, {}_0T_2 - {}_2S_1, {}_0S_3$  are combined into a super-multiplet, spectral differences can reach  $\sim 25$  per cent in the frequency windows of  ${}_0S_2$  and  ${}_0S_3$ . This illustrates that degenerate perturbation theory is no longer applicable whenever frequency perturbations are not first-order perturbations around the chosen fiducial frequency; quantitatively, a  $\sim 15$  per cent deviation from a fiducial frequency (e.g. the frequency of  ${}_0S_3$  relative to the average frequency of the super-multiplet ( ${}_0S_2 - {}_0T_2 - {}_2S_1 - {}_0S_3$ )) can give rise to notable differences in spectra.

### 3.5 Effect of eigensolution renormalization

We have seen that the proper normalization of the eigenfunctions of a rotating, anelastic Earth model is given by eq. (18). In this section, we examine the consequences of improperly normalizing the modes of a rotating, anelastic Earth model according to

$$\bar{\mathbf{q}}^T \mathbf{q} = 1, \quad (93)$$

which is the normalization used for a nonrotating, elastic, spherical Earth model. We calculate wideband spectra for all modes below 3 mHz and normalize them according to eqs (18) and (93), respectively. In Fig. 6(d), we compare wideband spectra for all modes improperly normalized according to eq. (93) with wideband spectra properly normalized according to eq. (18) as the reference. The difference accessed by calculating variance reduction (eq. 88) is at most  $\sim 1$  per cent, and we conclude that eq. (93) is adequate for normalizing eigensolutions on a rotating, anelastic and aspherical Earth model.

## 4 CONCLUSIONS

We reduce the equations of motion of a rotating, anelastic Earth model to quadratic left and right eigenvalue problems based on either real or complex spherical harmonics. The difficult-to-solve left eigenvalue problems may be transformed into auxiliary right eigenvalue problems. The choice of basis yields different symmetries of the coupling matrices, which result in complementary algebraic equations of motion. Either approach involves the introduction of an ‘anti-Earth’ with the opposite sense of rotation to the real Earth. The acceleration induced by an earthquake may be expressed in terms of the normal modes of the Earth and the anti-Earth. An expansion of these modes in the known modes of a spherically symmetric Earth model based on the Rayleigh–Ritz method results in an algebraic expression for the acceleration in terms of (large) coupling matrices.

We investigated various practical implementations of the Rayleigh–Ritz method. Wideband coupling involves coupling all modes below a certain frequency and is the most accurate—and also the most expensive—implementation of modes coupling. Narrowband coupling groups nearby modes into clusters and restricts coupling to the singlets that constitute the multiplets in the group, thereby reducing the size of the coupling matrices and the cost of the calculation. self coupling further restricts mode coupling to

the singlets within a target multiplet. Quasi-degenerate perturbation theory and various approximations to the frequency dependence of the potential energy, Coriolis and kinetic energy matrices reduce mode coupling to smaller and faster linear eigenvalue problems.

Compared to wideband coupling, self coupling—also referred to as the isolated-multiplet approximation—is only marginally acceptable at frequencies less below  $\sim 1.5$  mHz, and even then it fails when toroidal and spheroidal modes are in close proximity. Above 1.5 mHz, the self coupling approximation is unacceptable. Narrowband coupling performs only marginally better than self coupling below  $\sim 1.5$  mHz, but is a better approximation than self coupling at frequencies between 1.5 mHz and 3 mHz. Nevertheless, spectral errors due to narrowband coupling (below 3 mHz) and self coupling (below 1.5 mHz) are  $\sim 6$  per cent on average and can be as large as 10 per cent. The necessity of using wideband-coupling scheme rather than narrowband coupling and/or self coupling has been advocated in earlier studies of Deuss & Woodhouse (2001), Andrews *et al.* (2006), Irving *et al.* (2008), and Al-Attar *et al.* (2012).

Below 3 mHz, the effects of physical dispersion can be safely approximated based on either a fiducial frequency approximation or a quadratic approximation of the logarithmic dispersion associated with the absorption-band model. Approximations to the frequency dependence of the Coriolis matrix lead to  $\sim 6$  per cent errors in mode spectra for the gravest modes. Therefore, solving a quadratic eigenvalue problem is essential for acquiring accurate spectra at very low frequencies. Finally, neglecting the proper renormalization of the modes of a rotating, anelastic Earth model introduces only modest errors, up to 1 per cent for the gravest mode  ${}_0S_2$ .

## ACKNOWLEDGEMENTS

We welcome the comments and suggestions of the editor Michael Ritzwoller, David Al-Attar and an anonymous reviewer, which helped to improve the manuscript. HY also thanks Shu-Huei Hung and Li Zhao for discussions and Jose E. Roman for inspiring the idea of auxiliary right eigenproblems. Numerical simulations for this article were performed on a Dell cluster built and maintained by the Princeton Institute for Computational Science & Engineering (PIC-SciE). Figures were produced based on the Generic Mapping Tool (Wessel *et al.* 2013). The open source seismic measurement software package FLEXWIN used for this research is freely available for download via the Computational Infrastructure for Geodynamics (CIG; [geodynamics.org](http://geodynamics.org)). HY was supported by National Science Council of Taiwan (NSC) grant 102-2917-I-564-063 during her stay at Princeton University. This research was further supported by NSF grants 1063057 and 1112906 and NSC grants 102-2116-M-002-025 and 103-2811-M-002-223.

## REFERENCES

- Al-Attar, D., Deuss, A. & Woodhouse, J., 2012. Calculation of normal mode spectra in laterally heterogeneous earth models using an iterative direct solution method, *Geophys. J. Int.*, **189**, 1038–1046.
- Andrews, J., Deuss, A. & Woodhouse, J., 2006. Coupled normal-mode sensitivity to inner-core shear velocity and attenuation, *Geophys. J. Int.*, **167**(1), 204–212.
- Dahlen, F.A., 1968. The normal modes of a rotating, elliptical Earth, *Geophys. J. R. astr. Soc.*, **16**, 329–367.
- Dahlen, F.A., 1969. The normal modes of a rotating, elliptical Earth – II Near-resonance multiplet coupling, *Geophys. J. R. astr. Soc.*, **18**, 397–436.
- Dahlen, F.A., 1981. The free oscillations of an anelastic aspherical earth, *Geophys. J. R. astr. Soc.*, **66**, 1–22.
- Dahlen, F.A., 1987. Multiplet coupling and the calculation of synthetic long-period seismograms, *Geophys. J. R. astr. Soc.*, **91**, 241–254.
- Dahlen, F.A. & Smith, M.L., 1975. The influence of rotation on the free oscillations of the Earth, *Phil. Trans. R. Soc. Lond., A*, **275**, 583–627.
- Dahlen, F.A. & Tromp, J., 1998. *Theoretical Global Seismology*, Princeton Univ. Press.
- Deuss, A. & Woodhouse, J.H., 2001. Theoretical free-oscillation spectra: the importance of wide band-coupling, *Geophys. J. Int.*, **146**, 833–842.
- Deuss, A. & Woodhouse, J.H., 2004. Iteration method to determine the eigenvalues and eigenvectors of a target multiplet including full mode coupling, *Geophys. J. Int.*, **159**, 326–332.
- Deuss, A., Irving, J.C.E. & Woodhouse, J.H., 2010. Regional variation of inner core anisotropy from seismic normal mode observations, *Science*, **328**, 1018–1020.
- Deuss, A., Ritsema, J. & van Heijst, H., 2013. A new catalogue of normal-mode splitting function measurements up to 10 mHz, *Geophys. J. Int.*, **193**, 920–937.
- Durek, J.J. & Ekström, G., 1996. A radial model of anelasticity consistent with long-period surface-wave attenuation data, *Bull. seism. Soc. Am.*, **86**, 144–158.
- Dziewonski, A.M. & Anderson, D.L., 1981. Preliminary reference Earth model, *Phys. Earth planet. Int.*, **25**(4), 297–356.
- Giardini, D., Li, X.-D. & Woodhouse, J.H., 1988. Splitting functions of long-period normal-modes of the Earth, *J. geophys. Res.*, **93**(B11), 13 716–13 742.
- Gilbert, F., 1970. Excitation of the normal modes of the earth by earthquakes, *Geophys. J. R. astr. Soc.*, **22**, 223–226.
- Hara, T., Tsuboi, S. & Geller, R. J., 1993. Inversion for laterally heterogeneous upper mantle S-wave velocity structure using iterative waveform inversion, *Geophys. J. Int.*, **115**, 667–698.
- Henson, I.H., 1989. Multiplet coupling of the normal modes of an elliptical, transversely isotropic earth, *Geophys. J. Int.*, **98**, 457–459.
- Hernandez, V., Roman, J. E. & Vidal, V., 2005. SLEPC: A scalable and flexible toolkit for the solution of eigenvalue problem, *ACM Trans. Math. Softw.*, **31**(3), 351–362.
- Irving, J.C.E., Deuss, A. & Andrews, J., 2008. Wide-band coupling of Earth's normal modes due to anisotropic inner core structure., *Geophys. J. Int.*, **174**(3), 919–929.
- Ishii, M. & Dziewonski, A.M., 2002. The innermost inner core of the earth: Evidence for a change in anisotropic behavior at the radius of about 300 km, *Proc. Natl. Acad. Sci. USA*, **99**(22), 14 026–14 030.
- Ishii, M. & Tromp, J., 1999. Normal-mode and free-air gravity constraints on lateral variations in velocity and density of the Earth's mantle, *Science*, **285**, 1231–1236.
- Kanamori, H. & Anderson, D. L., 1977. Importance of physical dispersion in surface wave and free oscillation problems: review, *Rev. Geophys. Space Phys.*, **15**, 105–112.
- Laske, G., Masters, G. Ma, Z. & Pasyanos, M., 2013. Update on CRUST1.0 - A 1-degree global model of Earth's crust, *Geophys. Res. Abstracts*, **15**, Abstract EGU2013-2658.
- Lognonné, P., 1991. Normal modes and seismograms in an anelastic rotating Earth, *J. Geophys. Res.*, **96**(B12), 20 309–20 319.
- Luh, P.C., 1974. Normal modes of a rotating, self-gravitating inhomogeneous Earth, *Geophys. J. R. astr. Soc.*, **38**, 187–224.
- Maggi, A., Tape, C., Chen, M., Chao, D. & Tromp, J., 2009. An automated time-window selection algorithm for seismic tomography, *Geophys. J. Int.*, **178**, 257–281.
- Masters, G., Barmine, M. & Kientz, S., 2007. Mineos user manual, in *Computational Infrastructure for Geodynamics*, Calif. Inst. of Technol., Pasadena.
- Masters, G., Park, J. & Gilbert, F., 1983. Observations of coupled spheroidal and toroidal modes, *J. geophys. Res.*, **88**(10), 285–298.
- Millot-Langet, R., Clévéde, E. & Lognonné, P., 2003. Normal modes and long period seismograms in a 3D anelastic elliptical rotating Earth, *Geophys. Res. Lett.*, **30**(5), 1202, doi:10.1029/2002GL016257.

- Mochizuki, E., 1986. The free oscillations of an anisotropic and heterogeneous Earth, *Geophys. J. R. astr. Soc.*, **86**, 167–176.
- Nowick, A.S. & Berry, B.S., 1972. *Anelastic Relaxation in Crystalline Solids*, Academic Press.
- Park, J., 1987. Asymptotic coupled-mode expressions for multiplet amplitude anomalies and frequency shifts on an aspherical earth, *Geophys. J. R. astr. Soc.*, **90**, 129–170.
- Park, J., 1990. The subspace projection method for constructing coupled-mode synthetic seismograms, *Geophys. J. Int.*, **101**, 111–123.
- Park, J. & Gilbert, F., 1986. Coupled free oscillations of an aspherical, dissipative, rotating Earth: Galerkin theory, *J. geophys. Res.*, **91**(B7), 7241–7260.
- Resovsky, J. & Ritzwoller, M., 1998. New and refined constraints on three-dimensional Earth structure from normal modes below 3 mHz, *J. geophys. Res.*, **103**(B1), 783–810.
- Ritsema, J., van Heijst, H.J. & Woodhouse, J.H., 1999. Complex shear wave velocity structure imaged beneath Africa and Iceland, *Science*, **286**, 1925–1928.
- Roman, J.E., Campos, C., Romero, E. & Tomas, A., 2014. *SLEPc Users Manual, Tech. Rep. DSIC-II/24/02–Revision 3.5*, Universitat Politcnica de Valncia.
- Saad, Y., 2003. *Iterative Methods for Sparse Linear System*, 2nd edn, Society for Industrial and Applied Mathematics.
- Saad, Y. & Schultz, M.H., 1986. GMRES: A generalized minimal residual algorithm for solving nonsymmetric linear systems, *SIAM J. Sci. Stat. Comput.*, **7**(3), 856–869.
- Saito, M., 1967. Excitation of free oscillations and surface waves by a point source in a vertically heterogeneous Earth, *J. geophys. Res.*, **72**(14), 3689–3699.
- Shibata, N., Suda, N. & Fukao, Y., 1990. The matrix element for a transversely isotropic Earth model, *Geophys. J. Int.*, **100**(5), 315–318.
- Stewart, G.W., 2001. A Krylov–Schur algorithm for large eigenproblems, *SIAM J. Matrix Anal. Appl.*, **23**(3), 601–614.
- Tanimoto, T., 1986. Free oscillations of a slightly anisotropic Earth, *Geophys. J. R. astr. Soc.*, **87**, 493–517.
- Tromp, J. & Dahlen, F.A., 1990. Summation of the Born series for the normal modes of the Earth, *Geophys. J. Int.*, **121**, 963–968.
- Um, J. & Dahlen, F.A., 1992. Normal mode multiplet coupling on an aspherical anelastic Earth, *Geophys. J. Int.*, **111**, 11–31.
- van der Vorst, H.A., 1992. Bi-CGSTAB: a fast and smoothly converging variant of Bi-CG for the Solution of nonsymmetric linear systems, *SIAM J. Sci. Stat. Comput.*, **13**(2), 631–644.
- Wahr, J.M., 1981. A normal mode expansion for the forced response of a rotating earth, *Geophys. J. R. astr. Soc.*, **64**, 651–675.
- Wessel, P., Smith, W.H.F., Scharroo, R., Luis, J.F. & Wobbe, F., 2013. Generic Mapping Tools: improved version released, *EOS, Trans. Am. geophys. Un.*, **94**, 409–410.
- Woodhouse, J.H., 1980. The coupling and attenuation of nearly resonant multiplets in the Earth’s free oscillation spectrum, *Geophys. J. Int.*, **61**, 261–283.
- Woodhouse, J.H., 1988. The calculation of the eigenfrequencies and eigenfunctions of the free oscillations of the Earth and Sun, in *Seismological Algorithms: Computational Methods and Computer Programs*, pp. 321–370, ed. Doornbos, D.J., Academic Press.
- Woodhouse, J.H. & Dahlen, F.A., 1978. The effect of a general aspherical perturbation on the free oscillations of the Earth, *Geophys. J. R. astr. Soc.*, **53**, 335–354.
- Zurn, W., Laske, G., Widmer-Schmidrig, R. & Gilbert, F., 2000. Observation of Coriolis coupled modes below 1 mHz, *Geophys. J. Int.*, **143**, 113–118.

## APPENDIX: DERIVATION BASED ON THE INNER PRODUCT

Following Dahlen & Tromp (1998), we determined the response of a rotating, anelastic Earth model based on the duality product eq. (7). In this appendix, we demonstrate that the response can

**Table A1.** Eigensolutions and eigenfrequencies for the Earth and anti-Earth motivated by the inner product eq. (8).

	$\nu$	$-\nu^*$
Earth	$\mathbf{s}$	$\mathbf{s}^*$
Anti-Earth	$\underline{\mathbf{s}}^* = \bar{\mathbf{s}}$	$\underline{\mathbf{s}} = \bar{\mathbf{s}}^*$

also be determined based on the inner product eq. (8). Note that the inner product of two vectors  $\mathbf{u}$  and  $\mathbf{u}$  may be expressed as the duality product of  $\mathbf{u}^*$  and  $\mathbf{v}$ , that is

$$\langle \mathbf{u}, \mathbf{v} \rangle = [\mathbf{u}^*, \mathbf{v}]. \quad (\text{A1})$$

Unlike the duality product eq. (7), the inner product eq. (8) may be used to define the (positive-definite) norm of a vector, that is

$$\|\mathbf{u}\|^2 = \langle \mathbf{u}, \mathbf{u} \rangle = \int_{\oplus} \rho \mathbf{u}^*(\mathbf{x}) \cdot \mathbf{u}(\mathbf{x}) dV. \quad (\text{A2})$$

Let us start with the momentum equation for the actual Earth (eq. 1), where  $\mathbf{s}$  is the eigensolution with eigenfrequency  $\nu$ . Due to the antisymmetry of the Coriolis operator  $i \boldsymbol{\Omega} \times$  and the symmetry of the gravitational-elastic operator  $\mathcal{H}(\nu)$ , we can easily demonstrate that a general vector  $\underline{\mathbf{s}}$  satisfies the following relations with the displacement  $\mathbf{s}$ :

$$\langle \underline{\mathbf{s}}, \mathbf{s} \rangle = \langle \mathbf{s}, \underline{\mathbf{s}}^* \rangle, \quad (\text{A3})$$

$$\langle \underline{\mathbf{s}}, \mathcal{H}(\nu) \mathbf{s} \rangle = \langle \mathcal{H}^*(\nu) \underline{\mathbf{s}}, \mathbf{s} \rangle = \langle \mathbf{s}, \mathcal{H}^*(\nu) \underline{\mathbf{s}}^* \rangle, \quad (\text{A4})$$

$$\langle \underline{\mathbf{s}}, i \boldsymbol{\Omega} \times \mathbf{s} \rangle = \langle i \boldsymbol{\Omega} \times \underline{\mathbf{s}}, \mathbf{s} \rangle = \langle \mathbf{s}, i \boldsymbol{\Omega} \times \underline{\mathbf{s}}^* \rangle. \quad (\text{A5})$$

Analogous to eq. (13), the action  $\underline{\mathcal{I}}$  may be defined by taking the inner product of  $\underline{\mathbf{s}}$  with eq. (1):

$$\underline{\mathcal{I}} = \frac{1}{2} \{ \langle \underline{\mathbf{s}}, \mathcal{H}(\nu) \mathbf{s} \rangle + 2\nu \langle \underline{\mathbf{s}}, i \boldsymbol{\Omega} \times \mathbf{s} \rangle - \nu^2 \langle \underline{\mathbf{s}}, \mathbf{s} \rangle \}. \quad (\text{A6})$$

Using relationships eqs (A3)–(A5) and eq. (2), it is readily shown that the action eq. (A6) is stationary ( $\delta \underline{\mathcal{I}} = 0$ ) with respect to perturbations  $\delta \underline{\mathbf{s}}$  and  $\delta \mathbf{s}$  if

$$\mathcal{H}(\nu) \mathbf{s} + 2i\nu \boldsymbol{\Omega} \times \mathbf{s} - \nu^2 \mathbf{s} = \mathbf{0}, \quad (\text{A7})$$

$$\mathcal{H}(-\nu^*) \underline{\mathbf{s}} - 2(-\nu^*) i \boldsymbol{\Omega} \times \underline{\mathbf{s}} - (-\nu^*)^2 \underline{\mathbf{s}} = \mathbf{0}. \quad (\text{A8})$$

We conclude that  $\underline{\mathbf{s}}$  is a solution to the anti-earth equation of motion eq. (3) with eigenfrequency  $-\nu^*$ . This solution should be contrasted with the anti-Earth eigensolution  $\bar{\mathbf{s}}$  with eigenfrequency  $\nu$ . Upon taking the complex conjugate of eq. (A8), we find that

$$\mathcal{H}(\nu) \underline{\mathbf{s}}^* - 2\nu i \boldsymbol{\Omega} \times \underline{\mathbf{s}}^* - \nu^2 \underline{\mathbf{s}}^* = \mathbf{0}, \quad (\text{A9})$$

and upon comparison of this result with eq. (3) we recognize that

$$\underline{\mathbf{s}} = \bar{\mathbf{s}}^*, \quad (\text{A10})$$

and thus  $\underline{\mathbf{s}}^* = \bar{\mathbf{s}}$  with corresponding eigenfrequency  $\nu$ , as summarized in Table A1.

Using the relationship  $\underline{\mathbf{s}}^* = \bar{\mathbf{s}}$ , it is readily shown that  $\underline{\mathcal{I}} = \bar{\mathcal{I}}$ . Likewise, the eigensolution normalization eq. (10) may be expressed as

$$\langle \underline{\mathbf{s}}, \mathbf{s} \rangle - \nu^{-1} \langle \underline{\mathbf{s}}, i \boldsymbol{\Omega} \times \mathbf{s} \rangle - \frac{1}{2} \nu^{-1} \langle \underline{\mathbf{s}}, \partial_\nu \mathcal{H}(\nu) \mathbf{s} \rangle = 1, \quad (\text{A11})$$

and the Green’s tensor eq. (50) may be written in the form

$$\mathbf{G}(\mathbf{x}_r, \mathbf{x}_s; t) = \text{Re} \sum_k (i\nu_k)^{-1} \mathbf{s}_k(\mathbf{x}_r) \underline{\mathbf{s}}_k^*(\mathbf{x}_s) e^{i\nu_k t}. \quad (\text{A12})$$

Assuming that

$$\mathbf{s} = \sum_s q_s \mathbf{s}_s, \tag{A13}$$

and

$$\underline{\mathbf{s}} = \sum_s \underline{q}_s \mathbf{s}_s, \tag{A14}$$

where  $\mathbf{s}_s$  denote the known spherical Earth reference modes, we can express the action eq. (A6) in the algebraic form

$$\mathcal{I} = \underline{\mathbf{q}}^H [\mathbf{V}(v) + 2v\mathbf{W} - v^2\mathbf{T}] \mathbf{q}, \tag{A15}$$

and its stationarity implies the left and right eigenvalue problems

$$\underline{\mathbf{q}}^H [\mathbf{V}(v) + 2v\mathbf{W} - v^2\mathbf{T}] = \mathbf{0}, \tag{A16}$$

$$[\mathbf{V}(v) + 2v\mathbf{W} - v^2\mathbf{T}] \mathbf{q} = \mathbf{0}, \tag{A17}$$

respectively. The normalization of the eigensolution (eq. A11) becomes

$$\underline{\mathbf{q}}^H [\mathbf{T} - v^{-1}\mathbf{W} - \frac{1}{2} v^{-1} \partial_v \mathbf{V}(v)] \mathbf{q} = 1. \tag{A18}$$

Finally, the acceleration may be

$$a(t) = \text{Re} [\mathbf{r}'^H \exp(i\mathbf{N}t) \mathbf{s}'], \tag{A19}$$

where we have introduced the transformed receiver and source vectors

$$\mathbf{r}' = \mathbf{Q}^H \mathbf{r}^*, \tag{A20}$$

$$\mathbf{s}' = \underline{\mathbf{Q}}^H \mathbf{s}. \tag{A21}$$

The matrices  $\mathbf{Q}$  and  $\underline{\mathbf{Q}}$  have the eigenvectors  $\mathbf{q}$  and  $\underline{\mathbf{q}}$  as their respective columns.